Effect of surface stress induced curvature on the eigenfrequencies of microcantilever plates

Cite as: AIP Advances **8**, 105213 (2018); https://doi.org/10.1063/1.5053561
Submitted: 23 August 2018 . Accepted: 02 October 2018 . Published Online: 10 October 2018

J. J. Ruz, V. Pini, O. Malvar, P. M. Kosaka, M. Calleja, and J. Tamayo

Effect of surface stress induced curvature on the eigenfrequencies of microcantilever plates

J. J. Ruz, V. Pini, O. Malvar, P. M. Kosaka, M. Calleja, and J. Tamayo[a]
Instituto de Micro y Nanotecnología, IMN-CNM, CSIC (CEI UAM+CSIC), Isaac Newton, 8, E-28760 Tres Cantos, Madrid, Spain

(Received 23 August 2018; accepted 2 October 2018; published online 10 October 2018)

Ultrasensitive physical, chemical and biological sensors have emerged in the last decade based on the measurement of the eigenfrequencies of micro- and nanosized cantilever plates. Surface stress is omnipresent in these devices due to a variety of factors such as the fabrication process, temperature variations and analyte adsorption. How surface stress influences on the eigenfrequencies of cantilever plates has remained as an unsolved question in physics that has raised a long debate since first experiments in 1975. Recent theoretical models have shed light on the role of the net surface stress. Still, there exists a discrepancy between theory and some experimental reports, affecting to the capability for quantification of these sensors. In this Letter, we present a theoretical framework that demonstrates that the cantilever bending due to differential surface stress between opposite faces of the cantilever, a neglected effect in classical beam theory, plays a relevant role in the stiffness and eigenfrequencies of cantilevers. We develop a new theoretical framework that provides analytical equations that accurately describe the effect of surface stress on the first three vibration modes of cantilevers. Our findings provide the final piece of the puzzle for solving this long-standing problem in physics. https://doi.org/10.1063/1.5053561

I. INTRODUCTION

Micro- and nano-cantilevers are used as ultrasensitive mechanical sensors in a wide range of applications such as force microscopy/spectroscopy, biological sensors, optomechanics and accelerometers.[1–5] In the static operation mode, interaction forces are converted into displacements of the cantilever that are readily detected by optical or electrical methods. This method allows measuring the minuscule forces that govern biological interactions in single ligand-receptor force spectroscopy assays (normal forces)[2] as well as measuring the interactions within biomolecular films adsorbed on the cantilever's surface (in-plane forces).[4,6,7] In the dynamic mode, the fundamental resonance frequency of the cantilever is tracked in real-time for measuring the gradient of interaction forces,[8,9] molecular adsorption[10] and nanomechanical spectrometry of bioparticles.[11–15] The measurement of higher-order vibration modes has considerably gained interest due to the higher sensitivity and the capability for providing richer information when several eigenfrequencies are monitored.[11,12,14,16–18]

A subject of interest during the past four decades has been to know whether the omnipresent surface stress on cantilevers could modify their stiffness and eigenfrequencies.[10,19–22] Surface stress can be generated during the fabrication process and by molecular adsorption on the cantilever surface. In addition, cantilevers are commonly coated with a thin metallic film for improving the reflectivity or with active thin films for magnetic or piezoelectric actuation, which are stressed by small amounts of heat or by the actuation force, respectively.[23] The effect of surface stress was first studied by Lagowski et al in 1975 with the seminal work of Ref. 20. The authors found

[a]Corresponding author. E-mail Address: jtamayo@imm.cnm.csic.es

that the fundamental resonance frequency of GaAs cantilevers was extremely sensitive to surface stress. The experiments were interpreted with a taut string-like model, in which the tension is provided by the net surface stress along the cantilever's width. Only one year later, Gurtin et al rebutted this interpretation in a very short paper that reminds that in the framework of classical beam theory, strain-independent surface stress has no effect on the natural frequency of a thin cantilever beam.[19] In other words, cantilevers, unlike taut strings, have a free end to allow deformation for relieving the surface stress. Curiously, this confrontation between experimental reality and theoretical expectations has remained decades later.[24,25] Sader *et al.* reconciled experiments and theory by developing a cantilever plate model that takes into account the effect of the cantilever's width, traditionally ignored in the Euler-Bernoulli beam theory.[26] Sader's model reveals a region of unreleased in-plane stress in the vicinity of the supporting clamp that arises from the clamping restriction for in-plane displacements. The model was later improved and experimentally validated.[27,28] However, still there exist significant discrepancies between the theory and the experimental data.[10,20,25,29]

We believe that these discrepancies come from ignoring the cantilever bending induced by surface stress differences between the two cantilever faces.[4,30,31] This effect has been neglected as within the framework of linear elasticity theory, the bending state of a cantilever has not effect on its stiffness.[28,32] However, it has been observed that small amounts of transversal curvature in macroscopic thin plates can significantly increase the stiffness.[33] A few works have pointed out that the surface stress induced-curvature could significantly affect to the stiffness of cantilevers at micro- and nanoscales.[34–36] However, a theoretical explanation has remained elusive.

In this Letter, we develop a complete and novel theoretical framework for predicting the effect of surface stress induced curvature on the stiffness and eigenfrequencies of micro- and nanocantilevers. The theory accounts for three relevant effects previously ignored: i) internal stresses created by the two-dimensional curvature, ii) bending moment restriction by the clamping and iii) the effect of nonlinearities due to large static deformations.

II. RESULTS AND DISCUSSION

We study a cantilever plate with length L, width b and thickness h, Young's modulus E and Poisson's ratio ν (Fig. 1(a)). The cantilever is under uniform and isotropic surface stress loading on both faces, i.e., ${\sigma_s}^+$ and ${\sigma_s}^-$ on upper and lower faces. We define differential surface stress as $\Delta\sigma_s = {\sigma_s}^+ - {\sigma_s}^-$, and net surface stress as, $\sigma_s = {\sigma_s}^+ + {\sigma_s}^-$. The effect of net surface stress is depicted in Fig. 1(b). The unreleased in-plane stress near the clamping gives rise to a decrease of the resonance frequency, whereas the change of the cantilever dimensions due to the released surface stress makes the resonance frequency to increase.[26,27] Here, we study the effect of differential surface stress that induces a biaxial bending moment given by $M_s = \Delta\sigma_s \frac{h}{2}$ (Fig. 1(c)). The clamping restriction makes that the bending moment cannot be released near the clamping as it occurs with net surface stress. Thus, the cantilever deforms with isotropic and uniform curvature except near the clamping. We start the problem by studying the case of a cantilever plate that is unrestrained at all edges. Later, we will analyze the effect of the clamping restriction with the aid of numerical methods. The static displacement of the plate is then approximated by,

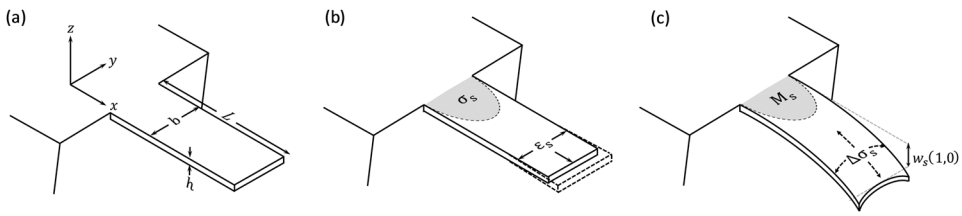

FIG. 1. Schematic of a cantilever plate showing: (a) the coordinate system and dimensions, (b) the unreleased in-plane stress (σ_s) and the strain due to total surface stress (ε_s), and (c) the unreleased bending moment (M_s) and bending due to differential surface stress ($\Delta\sigma_s$).

$$w_s(x,y) \cong \frac{1}{2}\kappa_s\left(x^2+y^2\right) \tag{1}$$

where $\kappa_s = \frac{6(1-\nu)\Delta\sigma_s}{Eh^2}$ is the surface stress induced curvature. Let $u|_{\omega_n}$, $v|_{\omega_n}$ and $w|_{\omega_n}$ be the amplitudes of the x and y in-plane displacements and z out-of-plane displacements at the *nth* order eigenfrequency respectively. These amplitudes can be approximated by second-order Taylor-expansion in the vertical coordinate z about the static displacement, referred to as $Z(x,y) = z - w_s(x,y)$,

$$u|_{\omega_n} = A\left\{u_{0,n}(x,y) - \frac{\partial\psi_n(x,y)}{\partial x}Z(x,y) + \frac{1}{2}u_{2,n}(x,y)Z(x,y)^2\right\} \tag{2}$$

$$v|_{\omega_n} = A\left\{v_{0,n}(x,y) - \frac{\partial\psi_n(x,y)}{\partial y}Z(x,y)\right\} \tag{3}$$

$$w|_{\omega_n} = A\left\{\psi_n(x,y) - \zeta(x,y)Z(x,y) + \frac{\nu}{2}\frac{\partial^2\psi_n(x,y)}{\partial x^2}Z(x,y)^2\right\} \tag{4}$$

where ψ_n is the *nth* order normalized eigenmode that describes the vibration-mode shape, A is an arbitrary amplitude factor and $u_{0,n}$, $u_{2,n}$, $v_{0,n}$ and ζ are unknown functions of our problem. The proposed displacement field departs with respect to classical Kirchhoff-Love plate theory in four relevant aspects.[32] First, the neutral plane is substituted by the curved surface, w_s of the bent plate. This apparently innocuous modification gives rise to the coupling of the dynamic and static stresses that plays a pivotal role in the stiffness of plates. Second, in-plane displacements of the mid surface are nonzero, albeit in-plane stresses are not exerted for the plate vibration. This effect is intimately linked to the previous effect. Third, a nonlinear term is included in the x-displacement that accounts for the effect of large static deflections. Fourth, the out-of-plane displacement comprises in addition to the eigenmode motion, first and second order terms in $Z(x,y)$. The first order term arises from the static deformation, whereas the second order term is just the result of the transverse strain associated to the bending strain. Unknown functions in our proposed displacements, $u_{0,n}$, $u_{2,n}$, $v_{0,n}$ and ζ are assumed to be linearly proportional to the maximum static deformation, thereby the displacements recover the classical Kirchhoff-Love plate theory expressions when $w_s(x,y) = 0$.

Next, we assume that the eigenmodes of the plate are negligibly modified by the static deformation and are approximated by,

$$\psi_n(x,y) = \phi_n(x) - \frac{1}{2}\nu\phi_n{}''(x)y^2 \tag{5}$$

where $\phi_n(x)$ represent the Euler-Bernoulli unidimensional eigenmodes and the second term accounts for the first-order deviation of the vibration of plates with respect to beams.

We proceed by applying linear elasticity relations to derive the strain tensor from the displacement vector given by $\left(u|_{\omega_n}, v|_{\omega_n}, w|_{\omega_n}\right)$, and calculating the force vector at each cross-section of the plate as well as the Lagrangian of the system. The unknown functions of the problem, $u_{0,n}$, $v_{0,n}$, $u_{2,n}$ and ζ (Eqs. (2)–(4)) are then obtained by applying equilibrium conditions and solving the Euler-Lagrange equations (supplementary material). We focus here on the resulting relative changes in the potential and kinetic energies due to the static deformation respectively given by,

$$\frac{\Delta U_n}{U_n} = \left\{\mu_n + \frac{(1-\nu)^2}{60}\left(\frac{b^4}{L^2h^2}\right)\right\}(\kappa_s L)^2 \tag{6}$$

$$\frac{\Delta T_n}{T_n} = \tau_n(\kappa_s L)^2 + 2\frac{\Delta\omega_n}{\omega_n} \tag{7}$$

The relative change of potential energy is proportional to the square of the dimensionless curvature, $\kappa_s L$ and accounts for the *nonlinear stiffening* of the cantilever due to the static deformation. It includes two terms, the first term proportionality constant, μ_n, is independent of the cantilever dimensions and arises from the geometric changes of the cantilever due to the static deformation and the nonlinear term in the x-displacement function, $u_{2,n}$. For the first three vibration modes $\mu_n = 0.46925, 0.38725, 0.35231$. The proportionality constant of the second term is mode-independent and rapidly increases as the plate is wider, $\sim\left(\frac{b}{L}\right)^4$, and thinner, $\sim\left(\frac{L}{h}\right)^2$. It arises from the in-plane stresses generated by the orthogonal coupling of the dynamic and static curvatures.[33] Hereinafter, the first two proportionality constants in the potential energy are referred to as *nonlinear beam*

stiffening and *nonlinear plate stiffening* coefficients. The relative change of kinetic energy includes two terms. The first term proportional to the square of the dimensionless curvature, $\kappa_s L$ accounts for the *nonlinear inertial* effect and is independent of the cantilever dimensions. Coefficient τ_n is result of the sum of the geometric effects on the effective cantilever mass and the increase of kinetic energy associated to the displacement in the x-direction. For, the first three vibration modes τ_n=*0.42867, 0.61831, 0.44593*. The second term in the kinetic energy is the unknown of our problem, the relative eigenfrequency shift. The relative changes in the eigenfrequencies are obtained by balancing the dynamic potential and kinetic energies,[13] $\frac{\Delta\omega_n}{\omega_n} = \frac{1}{2}\left(\frac{\Delta U_n}{U_n} - \frac{\Delta T_n}{T_n}\right)$.

We have compared our analytical equation of the eigenfrequency shifts with numerical simulations by the finite element method (FEM). The theory accurately describes the FEM results for narrow plates that satisfy $\frac{b}{L} < 0.2$. For wider plates, the model becomes less accurate and the deviation mostly arises from our estimation of the *nonlinear plate stiffening* coefficient. By careful examination of the numerical simulations, we have scrutinized the error induced by the adopted approximations. First source of error comes from the assumed vibration mode shape in Eq. (5). This is a good approximation for the fundamental vibration mode of cantilever plates with $\frac{b}{L} < 0.3$. However, the approximation becomes progressively less accurate for higher vibration modes and higher values of $\frac{b}{L}$.[18] This error can be reduced by including higher order terms in y in the eigenmode approximation at the expense of more complex expressions. We circumvent this difficulty by adding a term $\sim \left(\frac{b^6}{L^4h^2}\right)$ to the *nonlinear plate stiffening* factor, whose proportionality constant is obtained by fitting FEM calculations. Second source of error arises from neglecting the clamping restriction, which has two effects. First effect is of geometric nature, the static deformation $w_s(x, y)$ is not a paraboloid with uniform and isotropic curvature as approximated in Eq. (1). Although, there is not an exact analytical solution to this problem, we know that the transversal curvature is zero in the clamping and exponentially increases up to the asymptotic value with a characteristic length given by the cantilever's width.[31] The *clamping geometric effect* is here included by replacing the cantilever's width b by $be^{-c\frac{b}{L}}$ in the *nonlinear plate stiffening* factor, where $c \cong 0.7745$ is obtained by fitting the numerical results. Second effect of the clamping arises from the unreleased transversal bending moment near the clamping referred here to as *clamping stress effect* (Fig. 1(b)). By careful examination of the numerical simulations, we find that this effect induces *plate softening* and it can be simply accounted by replacing the biaxial prefactor by $(1-\nu)^2 - 2\nu$. Including all these corrections, the eigenfrequency shift is given by,

$$\frac{\Delta\omega_n}{\omega_n} = \left\{\alpha_n + \frac{1}{120}\left(\frac{b^4 e^{-4c\frac{b}{L}}}{L^2h^2}\right)\left\{\left((1-\nu)^2 - 2\nu\right) + \lambda_n(\nu)\left(\frac{b^2 e^{-2c\frac{b}{L}}}{L^2}\right)\right\}\right\}(\kappa_s L)^2 \tag{8}$$

where $\lambda_n(\nu)$ for the first three vibration modes is given by,

$$\begin{pmatrix}\lambda_1\\ \lambda_2\\ \lambda_3\end{pmatrix} = \begin{pmatrix}-0.33 & 8.82 & -29.31\\ 10.83 & -26.77 & -11.45\\ 8.13 & -3.22 & -29.80\end{pmatrix}\begin{pmatrix}1\\ \nu\\ \nu^2\end{pmatrix} \tag{9}$$

Notice that the function $\lambda_n(\nu)$ breaks the mode degeneration of the *nonlinear plate stiffening* coefficient. The constant $\alpha_n = \frac{\mu_n - \tau_n}{2}$ is the result of the counterbalance between the *nonlinear beam stiffening* and *nonlinear inertial* effects that give positive and negative eigenfrequency shifts, respectively. This coefficient is positive for the first vibration mode ($\alpha_1 \approx 0.02029$), whereas is negative for the second and third vibration modes ($\alpha_2 \approx -0.11553$, $\alpha_3 \approx -0.04670$). The trend observed here is consistent with reports in which microcantilevers exhibited stiffening in the nonlinear frequency response of the fundamental mode, and softening in the second and third vibration modes.[37,38] The first term is referred hereinafter to as *nonlinear beam effect.* The second term in Eq. (8) accounts for the *nonlinear plate stiffening*.

For the sake of a better understanding, we will focus now on a microcantilever with length $L = 10\,\mu m$, thickness $h = 0.1\,\mu m$, Young's modulus $E = 169\,GPa$ and Poisson's ratio $\nu = 0.064$. The values of E and ν correspond to those of single-crystal silicon when the length and the width of the cantilever are in the 110 directions.[39] The first three eigenfrequencies are 1.35, 8.44 and 23.6 MHz, respectively. Left graph in Fig. 2 shows the relative shifts of the first three eigenfrequencies as a function of the cantilever width-to-length ratio for a fixed value of differential surface stress

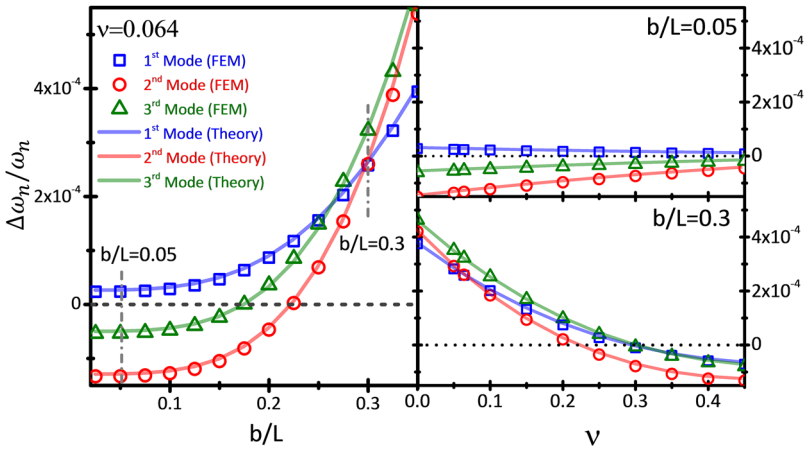

FIG. 2. Relative shift of the first three eigenfrequencies, $\Delta\omega_n/\omega_n$, of a cantilever subject to a differential surface stress of $1\,N/m$ as a function of the width-to-length ratio, $\frac{b}{L}$, and Poisson's ratio, ν. Fixed parameters of the calculations: $E = 169\,GPa$, $L = 10\,\mu m$ and $h = 0.1\,\mu m$. Symbols represent FEM data and lines represent our theoretical results, Eq. (8). Left graph shows, $\Delta\omega_n/\omega_n$ vs $\frac{b}{L}$ for $\nu = 0.064$. Right graph shows, $\Delta\omega_n/\omega_n$ vs ν for a narrow cantilever beam, $\frac{b}{L} = 0.05$, and for a wide cantilever plate $\frac{b}{L} = 0.3$.

$\Delta\sigma_s = 1\,N/m$. The curves show to regimes: the beam-like regime for $\frac{b}{L} \lesssim 0.1$ where the eigenfrequencies are dominated by the *nonlinear beam effect*, thus exhibiting little dependence on the cantilever's width, and the plate-like regime for $\frac{b}{L} \gtrsim 0.2$ where the effect of *nonlinear plate stiffening* becomes dominant and the eigenfrequencies rapidly increase as $\sim \left(\frac{b}{L}\right)^4$. In general, the transition between these two regimes occurs for $\frac{b}{L} \sim \sqrt{\frac{h}{L}}$. For the case examined here, the relative eigenfrequency shifts approximately are 20, -130 and -50 ppm in the beam-like regime, and can achieve more than 400 ppm in the plate-like regime. Since for the second and third vibration modes, the *nonlinear beam effect* gives negative eigenfrequency shifts, there exist a width where the *nonlinear beam effect* and *nonlinear plate stiffening* cancel each other, being insensitive to the surface stress. This occurs when $b \approx 2.25\,\mu m$ for the second vibration mode and $b \approx 1.8\,\mu m$ for the third vibration mode. Interestingly, this phenomenon can be used for uncoupling the effect of differential surface stress from other effects (mass and stiffness)[12] on the eigenfrequency shift.

Right graphs in Fig. 2 show the effect of Poisson's ratio on the fractional frequency shifts for a narrow cantilever beam, $\frac{b}{L} = 0.05$, and for a wide cantilever plate $\frac{b}{L} = 0.3$, keeping $\Delta\sigma_s = 1\,N/m$. In the limit of narrow cantilevers, the eigenfrequency shifts are independent of the Poisson's ratio for same values of cantilever bending. The dependence on the Poisson's ratio in this case, arises from the dependence of the cantilever curvature on the surface stress that is $\kappa_s \sim (1 - \nu)$. In the case of wide cantilever plates, Poisson's ratio strongly influences the frequency response. This comes from the dependence of the *nonlinear plate stiffening* on the Poisson's ratio that at first order scales as $\left((1-\nu)^2 - 2\nu\right)$, where the term -2ν arises from *clamping stress effect* described above. Interestingly, plate stiffening can turn into negative (softening) for Poisson ratios above a critical value that depends on the cantilever width. In our example (Fig. 2, right-bottom graph), the critical Poisson's ratio is 0.285, 0.220 and 0.297 for the first three vibration modes.

We now emphasize the accuracy of our model: the mean deviation between the results obtained by the analytical equation (8) in Fig. 2 and the FEM simulations is below 1% for the first two modes and 2% for the third mode for $\frac{b}{L} < 0.3$. For wider cantilevers, the error becomes significant for the second and third modes, being of about 3.7% and 7.3% at $\frac{b}{L} = 0.35$, repectively.

In Fig. 3, we compare the effects of differential surface stress ($\Delta\sigma_s$) (left graph) and net surface stress (σ_s) (right graph) for the first and second vibration modes. The surface stress loading on the top and bottom faces for these cases are ${\sigma_s}^+ = -{\sigma_s}^- = \frac{\sigma}{2}$ and ${\sigma_s}^+ = {\sigma_s}^- = \frac{\sigma}{2}$, respectively. In the practical case, in which surface stress is only acting on the upper face, $\Delta\sigma_s = \sigma_s = \frac{\sigma}{2}$, the resonance frequency shift can be calculated as the half sum of the two effects. The analysis is performed for a narrow cantilever beam, $b = 0.5\,\mu m$ and for a wide cantilever plate $b = 3\,\mu m$ and three Poisson's

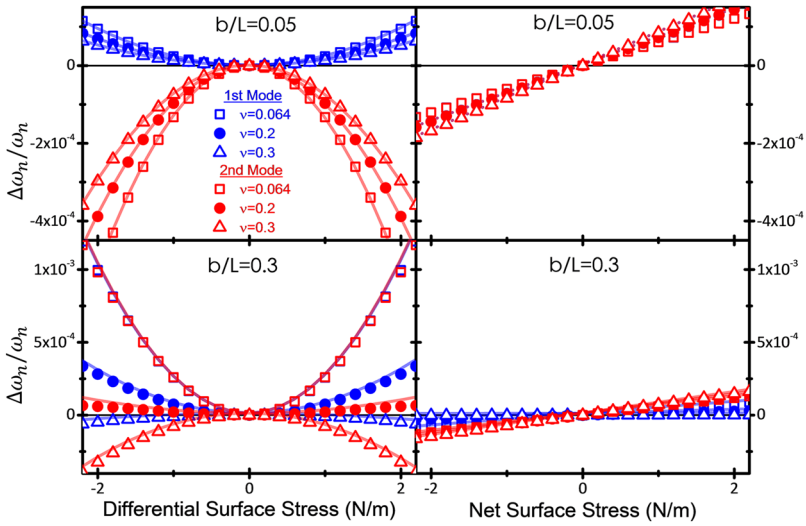

FIG. 3. Relative frequency shifts of the first (blue) and second vibration (red) modes of a microcantilever as a function of differential surface stress (left) and net surface stress (right) for $\frac{b}{L} = 0.05$ (top) and $\frac{b}{L} = 0.3$ (bottom) Symbols represent FEM data and lines represent our theoretical results, Eq. (8). For net surface stress effect only FEM data is shown. The microcantilever is 10 μm long and 0.1 μm thick. The data is shown for several Poisson's ratio values: 0.064, 0.2 and 0.3. The relative frequency shifts of the first and second vibration modes due to net surface stress overlap for $\frac{b}{L} = 0.05$ (right-top graph) and almost overlap for $\frac{b}{L} = 0.3$ and ν=0.064 when differential surface stress varies (left-bottom graph).

ratio values: 0.064, 0.2 and 0.3. The most remarkable difference between these two effects is that the resonance frequency shift goes as the square of differential surface stress whereas is linear with the net surface stress. For $\frac{b}{L} = 0.05$, $\Delta\sigma_s$ induces positive and negative eigenfrequency shifts in the first and second vibration modes, respectively. The eigenfrequency shifts of the second vibration mode are significantly larger than those of the first vibration mode. On the contrary, the eigenfrequency shift induced by net surface stress is independent of the vibration mode for the first three vibration modes (third vibration mode data not shown). In the regime of narrow beams, the main effect of net surface stress is the modification of the cantilever length (*geometric effect*), giving rise to[27] $\Delta\omega_n/\omega_n \approx (1+2\nu)\frac{\sigma_s}{Eh}$. The magnitude of both effects, differential and total surface stress is comparable in narrow beams for surface stress values of $\sim 1\,N/m$. Cantilever plates with $\frac{b}{L} = 0.3$ exhibit a very different behavior. Differential surface stress can induce relative frequency shifts exceeding 10^{-3} for $\nu = 0.064$ that are significantly larger than those induced by net surface stress. The effect of differential surface stress mitigates as the Poisson's ratio increases and change of sign for $\nu = 0.3$. Net surface stress effect decreases in wide plates with respect to narrow beams, especially in the first vibration mode. This decrease arises from the unreleased stress near the clamping (Fig. 1(a)) that goes as[26] $\sim -\nu(1-\nu)\left(\frac{b}{L}\right)^3\left(\frac{L}{h}\right)^2\frac{\sigma_s}{Eh}$.

III. CONCLUSION

In conclusion, we have presented a novel theoretical framework that describes the effect of differential surface stress on the stiffness and eigenfrequencies of cantilevers. The theory accounts for linear and nonlinear effects previously ignored, providing a solid base to reformulate the results of classical beam theory. The results shown here, together with previous studies of the effect of net surface stress,[26,27] enable to provide a definitive answer to the long standing problem in physics initiated by Gurtin et al in 1976: the effect of surface stress on the natural frequency of thin crystals.[19]

SUPPLEMENTARY MATERIAL

See supplementary material for a more detailed derivation of the equations of this manuscript and for additional information about the finite element simulations.

ACKNOWLEDGMENTS

This study has been supported by European Union' s Horizon 2020 research and innovation programme under grant agreement No 731868 – VIRUSCAN and European Research Council grant 681275 – LIQUIDMASS- ERC- CoG-2015; by Spanish Ministry of Economy and Competitiveness (grant MAT2015-66904-R). PMK acknowledges financial support by Fundación General CSIC (ComFuturo Program).

[1] T. Ando, T. Uchihashi, and S. Scheuring, Chem. Rev. **114**(6), 3120 (2014).
[2] A. R. Bizzarri and S. Cannistraro, Chem. Soc. Rev. **39**(2), 734 (2010).
[3] M. Li, H. X. Tang, and M. L. Roukes, Nat. Nanotechnol. **2**(2), 114 (2007).
[4] J. Tamayo, P. M. Kosaka, J. J. Ruz, Á. San Paulo, and M. Calleja, Chem. Soc. Rev. **42**(3), 1287 (2013).
[5] P. Weber, J. Güttinger, A. Noury, J. Vergara-Cruz, and A. Bachtold, Nat. Commun. **7**, 12496 (2016).
[6] R. McKendry, J. Zhang, Y. Arntz, T. Strunz, M. Hegner, H. P. Lang, M. K. Baller, U. Certa, E. Meyer, and H.-J. Güntherodt, P. Natl. Acad. Sci. **99**(15), 9783 (2002).
[7] G. Wu, R. H. Datar, K. M. Hansen, T. Thundat, R. J. Cote, and A. Majumdar, Nat. Biotechnol. **19**(9), 856 (2001).
[8] T. R. Albrecht, P. Grütter, D. Horne, and D. Rugar, J. Appl. Phys. **69**(2), 668 (1991).
[9] M. Poggio and C. L. Degen, Nanotechnology **21**(34), 342001 (2010).
[10] T. Thundat, E. A. Wachter, S. L. Sharp, and R. J. Warmack, Appl. Phys. Lett. **66**(13), 1695 (1995).
[11] M. S. Hanay, S. Kelber, A. K. Naik, D. Chi, S. Hentz, E. C. Bullard, E. Colinet, L. Duraffourg, and M. L. Roukes, Nat. Nanotechnol. **7**(9), 602 (2012).
[12] O. Malvar, J. J. Ruz, P. M. Kosaka, C. M. Domínguez, E. Gil-Santos, M. Calleja, and J. Tamayo, Nat. Commun. **7**, 13452 (2016).
[13] J. J. Ruz, J. Tamayo, V. Pini, P. M. Kosaka, and M. Calleja, Sci. Rep. **4**, 6051 (2014).
[14] E. Sage, A. Brenac, T. Alava, R. Morel, C. Dupré, M. S. Hanay, M. L. Roukes, L. Duraffourg, C. Masselon, and S. Hentz, Nat. Commun. **6**, 6482 (2015).
[15] P. M. Kosaka, M. Calleja, and J. Tamayo, Semin. Cancer. Biol. **52**, 26 (2018).
[16] S. Dohn, R. Sandberg, W. Svendsen, and A. Boisen, Appl. Phys. Lett. **86**(23), 233501 (2005).
[17] A. Raman, S. Trigueros, A. Cartagena, A. P. Z. Stevenson, M. Susilo, E. Nauman, and S. A. Contera, Nat. Nanotechnol. **6**(12), 809 (2011).
[18] J. Tamayo, V. Pini, P. Kosaka, N. F. Martinez, O. Ahumada, and M. Calleja, Nanotechnology **23**(31), 315501 (2012).
[19] M. E. Gurtin, X. Markenscoff, and R. N. Thurston, Appl. Phys. Lett. **29**(9), 529 (1976).
[20] J. Lagowski, H. C. Gatos, and E. S. Sproles, Jr., Appl. Phys. Lett. **26**(9), 493 (1975).
[21] D. Lee, S. Kim, N. Jung, T. Thundat, and S. Jeon, J. Appl. Phys. **106**(2), 024310 (2009).
[22] M. L. C. De Laat, H. H. P. Garza, J. L. Herder, and M. K. Ghatkesar, J. Micromech. Microeng. **26**(6), 063001 (2016).
[23] N.-H. Zhang, Thin Solid Films **515**(23), 8402 (2007).
[24] P. Lu, H. P. Lee, C. Lu, and S. J. O'shea, Phys. Rev. B **72**(8), 085405 (2005).
[25] A. W. McFarland, M. A. Poggi, M. J. Doyle, L. A. Bottomley, and J. S. Colton, Appl. Phys. Lett. **87**(5), 053505 (2005).
[26] M. J. Lachut and J. E. Sader, Phys. Rev. Lett. **99**(20), 206102 (2007).
[27] R. B. Karabalin, L. G. Villanueva, M. H. Matheny, J. E. Sader, and M. L. Roukes, Phys. Rev. Lett. **108**(23), 236101 (2012).
[28] M. J. Lachut and J. E. Sader, Phys. Rev. B **85**(8), 085440 (2012).
[29] K. S. Hwang, K. Eom, J. H. Lee, D. W. Chun, B. H. Cha, D. S. Yoon, T. S. Kim, and J. H. Park, Appl. Phys. Lett. **89**(17), 173905 (2006).
[30] J. E. Sader, J. Appl. Phys. **89**(5), 2911 (2001).
[31] J. Tamayo, J. J. Ruz, V. Pini, P. Kosaka, and M. Calleja, Nanotechnology **23**(47), 475702 (2012).
[32] J. N. Reddy, *Theory and analysis of elastic plates and shells* (CRC press, 2006).
[33] V. Pini, J. J. Ruz, P. M. Kosaka, O. Malvar, M. Calleja, and J. Tamayo, Sci. Rep. **6**, 29627 (2016).
[34] A. Najafi Sohi and P. M. Nieva, J. Appl. Phys. **119**(4), 044503 (2016).
[35] V. Pini, J. Tamayo, E. Gil-Santos, D. Ramos, P. Kosaka, H.-D. Tong, C. van Rijn, and M. Calleja, Acs Nano **5**(6), 4269 (2011).
[36] U. Harms, L. Kempen, and H. Neuhäuser, Thin Solid Films **323**(1-2), 153 (1998).
[37] W. J. Venstra, H. J. R. Westra, and H. S. J. van der Zant, Appl. Phys. Lett. **97**(19), 193107 (2010).
[38] L. G. Villanueva, R. B. Karabalin, M. H. Matheny, D. Chi, J. E. Sader, and M. L. Roukes, Phys. Rev. B **87**(2), 024304 (2013).
[39] M. A. Hopcroft, W. D. Nix, and T. W. Kenny, J. Microelectromech. S. **19**(2), 229 (2010).